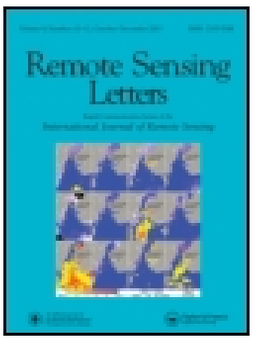

Remote Sensing Letters

ISSN: 2150-704X (Print) 2150-7058 (Online) Journal homepage: http://www.tandfonline.com/loi/trsl20

Unsupervised classification based on fuzzy c-means with uncertainty analysis

Qunming Wang & Wenzhong Shi

To cite this article: Qunming Wang & Wenzhong Shi (2013) Unsupervised classification based on fuzzy c-means with uncertainty analysis, Remote Sensing Letters, 4:11, 1087-1096, DOI: 10.1080/2150704X.2013.832842

To link to this article: http://dx.doi.org/10.1080/2150704X.2013.832842

Remote Sensing Letters, 2013
Vol. 4, No. 11, 1087–1096, http://dx.doi.org/10.1080/2150704X.2013.832842

Unsupervised classification based on fuzzy *c*-means with uncertainty analysis

QUNMING WANG and WENZHONG SHI*
Department of Land Surveying and Geo-Informatics, The Hong Kong Polytechnic University, Kowloon, Hong Kong

(*Received 26 March 2013; accepted 4 August 2013*)

Fuzzy *c*-means (FCM) is a widely used unsupervised classifier for remote sensing images. This letter presents an uncertainty analysis-based FCM (UAFCM) classification method. The uncertainty in this letter refers to the discriminative ability of class attributes in fuzzy classification on a per-pixel basis. UAFCM is performed by analysing the uncertainty in FCM classification result and reclassifying the pixels with large uncertainty. Specifically, the uncertainty in FCM classification is measured by entropy and a proposed square error-based criterion. A threshold value is then determined to recognize the pixels with large uncertainty, which are reclassified with spatial connectivity subsequently. Experiments on three remote sensing images show that the proposed UAFCM consistently obtains more accurate classification results than does FCM, and hence provides an effective new unsupervised classification method for remote sensing images.

1. Introduction

Remote sensing techniques have been used in many application fields such as agriculture, forestry, geology, and oceanology (Richards and Jia 2006, Wang *et al.* 2012). Extraction of land cover information from remote sensing images is usually accomplished by classification and it is one of the most important techniques in the field of remote sensing. There are three basic types of classification methods: supervised, unsupervised, and hybrid. Supervised classification requires training samples from each class to guide classification. Commonly used algorithms include minimum distance, maximum likelihood classification, artificial neural networks, support vector machines, etc. By contrast, unsupervised classification does not require training samples to label classes for pixels and classes are distinguished by exploiting spectral information of pixels. The hybrid classification is a combination of both supervised and unsupervised classification (Dopido *et al.* 2006).

Various algorithms have been developed for unsupervised classification including *k*-means clustering (Duda *et al.* 2001), iterative self-organizing data analysis techniques algorithm (Hall and Ball 1965), self-organizing maps (Bagan *et al.* 2005), and Markov random field (MRF) (Xu *et al.* 2013). In addition, artificial intelligence has also been employed for unsupervised classification such as genetic algorithms (Bandyopadhyay *et al.* 2007) and artificial immune system (Zhong *et al.* 2011). The core idea of unsupervised classification is to seek an optimal cluster centre for each

*Corresponding author. Email: lswzshi@polyu.edu.hk

class that has been artificially predefined by analysts. The classical k-means clustering is performed based on the assumption that a pixel only belongs to one cluster. As an extension of k-means clustering, fuzzy c-means (FCM) (Bezdek 1981) clustering provides soft clusters, where a pixel has a degree of membership in each cluster (Dopido *et al.* 2006). FCM has been widely applied for unsupervised classification of remote sensing images for many years.

Remote sensing process often includes data acquisition, image gaining, and interpretation. All of the involved instrumentations, techniques, and models in the three steps can lead to an uncertainty in remote sensing images interpretation (such as land cover classification) (Dehghan and Ghassemian 2006, Richards and Jia 2006). In remote sensing, measures such as the membership probability of a pixel for each class are often used as indicator of uncertainty in classification on a per-pixel basis (Brown *et al.* 2009). The outputs of FCM are essentially fuzzy class attribute values indicating membership probabilities, which have been hardened in conventional FCM results. These fuzzy outputs can provide information on uncertainty in FCM classification. For those pixels with large uncertainty in classification, reclassification of them by using other information is expected to obtain higher classification accuracy. Aiming at this issue, two problems need to be solved. One is for each pixel, how to determine whether the uncertainty in classification of it is large or not? The other is for pixels with large uncertainty in classification, how to perform reclassification?

In this letter, the classical FCM is enhanced by analysing uncertainty in FCM classification result and an uncertainty analysis-based FCM (UAFCM) classification method is proposed. UAFCM recognizes pixels with large uncertainty in traditional FCM classification result using a threshold value and performs reclassification for pixels with large uncertainty using spatial connectivity. In UAFCM, uncertainty in classification for each pixel is measured first based on two criteria: entropy (Foody 1995) and a proposed criterion based on square error. According to the estimated values measuring uncertainty for all pixels, a threshold value is determined. The pixels with large uncertainty are then identified using this threshold value. For each pixel with large uncertainty, reclassification is performed based on spatial connectivity, by which neighbouring pixels' class labels are considered. The main contributions of this letter are as follows:

1. Proposing an uncertainty analysis-based method for post-processing of conventional FCM classification.
2. Proposing a new criterion based on square error to quantify the uncertainty in fuzzy classification.

2. FCM

Suppose there are n test samples, $\boldsymbol{x}_1, \boldsymbol{x}_2, ..., \boldsymbol{x}_n$, and k is the number of clusters or classes. Define $u_{ij} \in [0, 1]$ as the membership probability of pixel $\boldsymbol{x}_j$ ($j = 1, 2, \ldots, n$) for the ith ($i = 1, 2, \ldots, k$) class. The goal of FCM is to obtain the matrix $\boldsymbol{U} = [u_{ij}]$ and the hard classification is achieved by assigning each pixel to the class with the highest membership probability. u_{ij} should satisfy

$$\sum_{i=1}^{k} u_{ij} = 1, \quad j = 1, 2, ..., n \tag{1}$$

The clustering is performed by minimizing

$$J(\boldsymbol{U}, \boldsymbol{V}) = \sum_{i=1}^{k} \sum_{j=1}^{n} u_{ij}^{m} \left\| \boldsymbol{x}_j - \boldsymbol{v}_i \right\|^2 \tag{2}$$

where $\boldsymbol{V} = [\boldsymbol{v}_1, \boldsymbol{v}_2, ..., \boldsymbol{v}_k]$ is a matrix composed of k vectors, each one containing the coordinates of a cluster centre. m is a weighting exponent and usually set to 2, a widely used value in many works.

The matrix $\boldsymbol{U}$ is randomly initialized with its elements falling within [0, 1] and meeting condition in equation (1), and updated iteratively to approach an optimum solution. During the iterations, the cluster centre for the ith class is updated by

$$\boldsymbol{v}_i = \frac{\sum_{j=1}^{n} u_{ij}^{m} \boldsymbol{x}_j}{\sum_{j=1}^{n} u_{ij}^{m}} \tag{3}$$

and the membership probability u_{ij} is updated correspondingly by

$$u_{ij} = \frac{1}{\sum_{t=1}^{k} \left(\frac{\left\| \boldsymbol{x}_j - \boldsymbol{v}_i \right\|}{\left\| \boldsymbol{x}_j - \boldsymbol{v}_t \right\|} \right)^{\frac{2}{m-1}}} \tag{4}$$

3. UAFCM

3.1 *Measurement of uncertainty*

First of all, it is essential to quantify the uncertainty in classification. The criterion for uncertainty should satisfy two basic conditions:

(i) The value is maximized when the membership probability of each class is partitioned evenly between all classes; and (ii) the value is minimized when the membership probability is associated entirely with one class (Foody 1995).

In this letter, the uncertainty in FCM classification is measured by two criteria, entropy and a proposed criterion based on square error.

3.1.1 Entropy. Entropy is widely used to measure uncertainty in remote sensing classification (Foody 1995, Dehghan and Ghassemian 2006, Brown *et al.* 2009). For a particular pixel, say $\boldsymbol{x}_j$, the uncertainty in classification quantified by entropy is

$$E_{\mathrm{EN}}^{0}(j) = -\sum_{i=1}^{k} u_{ij} \log_2 u_{ij} \tag{5}$$

The criterion in equation (5) satisfies the two basic conditions (i) and (ii), as mentioned in (Foody 1995, Dehghan and Ghassemian 2006, Brown *et al.* 2009). Each value estimated by equation (5) falls within the interval [0, $\log_2 k$] and it may be normalized by

$$E_{\mathrm{EN}}(j) = \frac{E_{\mathrm{EN}}^{0}(j)}{\log_2 k} \tag{6}$$

so that it falls within [0, 1].

3.1.2 Square error. The uncertainty in classification of $\boldsymbol{x}_j$ that is quantified by the proposed square error is

$$E_{\mathrm{SE}}^0(j) = -\sum_{i=1}^{k}\left(u_{ij} - \frac{1}{k}\right)^2 \tag{7}$$

Evidently, the criterion satisfies condition (i). As for condition (ii), it is also satisfied.

$$\begin{aligned} E_{\mathrm{SE}}^0(j) &= -\sum_{i=1}^{k}\left(u_{ij}^2 - \frac{2u_{ij}}{k} + \frac{1}{k^2}\right) = -\left[\left(\sum_{i=1}^{k} u_{ij}^2\right) - \frac{1}{k}\right] \geq -\left[\left(\sum_{i=1}^{k} u_{ij}\right) - \frac{1}{k}\right] \\ &= -\left(1 - \frac{1}{k}\right) \end{aligned} \tag{8}$$

From equation (8), we can see $E_{\mathrm{SE}}^0(j)$ has the minimum value $-(1 - \frac{1}{k})$. It is critical to demonstrate the assumption $E_{\mathrm{SE}}^0(j)$ reaches this minimum value when the membership probability is associated entirely with one class (i.e., condition (ii)). We provide the demonstration for this assumption here.

$$\begin{aligned} &E_{\mathrm{SE}}^0(j) = -\left(1 - \frac{1}{k}\right) \Rightarrow -\left[\left(\sum_{i=1}^{k} u_{ij}^2\right) - \frac{1}{k}\right] = -(1 - \frac{1}{k}) \Rightarrow \sum_{i=1}^{k} u_{ij}^2 = 1 \Rightarrow \sum_{i=1}^{k} u_{ij}^2 \\ &= \sum_{i=1}^{k} u_{ij} \quad \begin{array}{l} \Rightarrow \sum_{i=1}^{k}\left[u_{ij}(u_{ij} - 1)\right] = 0 \\ 0 \leq u_{ij} \leq 1 \Rightarrow u_{ij}(u_{ij} - 1) \leq 0 \end{array} \Bigg\} \Rightarrow u_{ij}(u_{ij} - 1) = 0, \text{for all } i \Rightarrow u_{ij} = \begin{cases} 1, i = i_0 \\ 0, i \neq i_0 \end{cases} \end{aligned} \tag{9}$$

This means only when the membership probability of a certain class (denoted as i_0 in equation (9)) is 1 (the membership probabilities of other classes are 0 in the meanwhile according to (1)), $E_{\mathrm{SE}}^0(j)$ reaches the minimum value. Therefore, condition (ii) is evidently satisfied for the proposed square error based criterion. $E_{\mathrm{SE}}^0(j)$ may be normalized by

$$E_{\mathrm{SE}}(j) = \frac{E_{\mathrm{SE}}^0(j) + \left(1 - \frac{1}{k}\right)}{1 - \frac{1}{k}} \tag{10}$$

to fall within [0, 1].

3.2 *Recognition of pixels with large uncertainty*

After the uncertainty for all n pixels in an image is quantified, we can obtain the mean and variance (denoted as $\overline{E}$ and σ, respectively) of the n values $E_1, E_2, ..., E_n$. A threshold can be generated from an empirical equation

$$\gamma = \overline{E} + \rho\sigma \tag{11}$$

where ρ is a constant. The threshold value is used to recognize those pixels with large uncertainty: if $E_j \geq \gamma$ (E_j can be calculated by equation (6) or equation (10)), then pixel j is considered as a pixel with large uncertainty in classification; otherwise, pixel j is recognized as a pixel with small uncertainty in classification.

3.3 *Reclassification of pixels with large uncertainty*

For those pixels with large uncertainty, reclassification is performed with the aid of spatial connectivity. According to spatial connectivity theory, most of the spatial objects are neighbourhood connected. That is, the centre pixel is the most likely to be of the class that has already been assigned to most of the neighbouring pixels.

The pixels with large uncertainty are marked as unlabelled ones first of all. For any unlabelled pixel, by searching its $W \times W$ neighbouring pixels, those already labelled pixels are recorded along with their class labels. Then, the unlabelled centre pixel will be allocated to the class that has already been assigned to the largest number of neighbouring pixels. If an unlabelled pixel is entirely surrounded by pixels with large uncertainty, the class with the highest membership is found out and recorded for each pixel in the $W \times W$ window at first and the unlabelled centre pixel will be labelled as the class with the largest vote in the local window. The whole process is terminated when all uncertain pixels are labelled.

The proposed UAFCM-based unsupervised classification method is a post-processing of conventional FCM classification. It can be easily realized by the remote sensing data analysts and easily coded in any computing language. Also, UAFCM is a very fast method. It is non-iterative (iterations in FCM are not considered) as reclassification of pixels with large uncertainty is a single-pass method. Different from some post-processing techniques, such as mode filtering (Evans and Nixon 1995), UAFCM only reclassifies uncertain pixels and updates their class labels. If some elongated features or small objects can be correctly classified by FCM, using those post-processing methods, these features may be smoothed or even lost. However, if pixels for these features are ones with small uncertainty, UAFCM will not update their labels and will retain these features as a result. This is an advantage of the proposed UAFCM.

4. Experimental results and analysis

In this section, experiments on three remote sensing images were carried out to validate the effectiveness and advantage of the proposed UAFCM. Five unsupervised classification methods were tested: FCM, FCM results with neighbourhood voting (FCMNV), MRF, UAFCM using entropy (FCMEN) and UAFCM using square error (FCMSE) to measure uncertainty. It took less than 2 seconds to run UAFCM after FCM on an Intel Core i7 Processor at 3.40-GHz with MATLAB 7.1 version.

4.1 *Data description*

The detailed information on three data sets for test is described as follows.

The Flightline C1 (FLC1) data set. FLC1 covers an agricultural district located in the southern part of Tippecanoe County (Zhong *et al.* 2011). A part of the data set (110 × 190 pixels) with 12 bands was used for test. The studied site mainly contains four vegetative species: red clover, oats, soy, and wheat. Three-band colour composite image of the studied site is shown in figure 1(*a*) and the ground reference data is shown in figure 1(*b*). The numbers of test samples of red clover, oats, soy, and wheat are 4370, 1296, 3446, and 2385, respectively.

The Hyperspectral Digital Imagery Collection Experiment (HYDICE) data set. The HYDICE airborne hyper-spectral data covers an area of the Washington, DC Mall (191 bands with a spatial resolution of 3 m) (Zhang *et al.* 2013). The studied area has 200 × 307 pixels and mainly covers five classes: tree, trail, road, grass, and roof. Figures 2(*a*) and (*b*) gives the information of the image. The numbers of

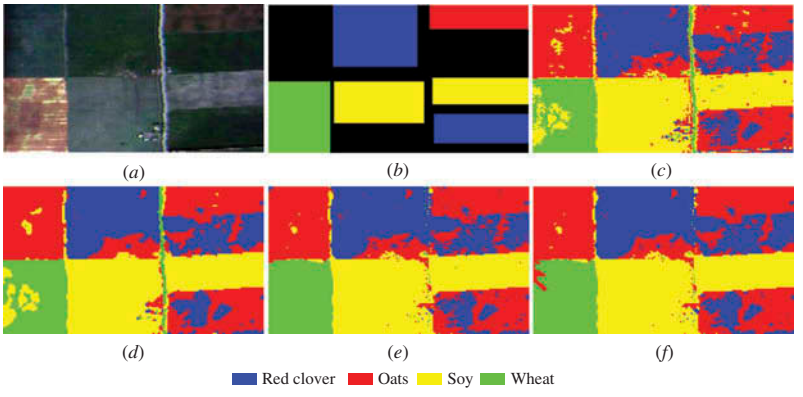

Figure 1. Results of FLC1 data set. (*a*) Three-band colour composite image (bands 9, 6, and 3 as RGB). (*b*) Ground truth. (*c*)–(*f*) FCM, FCMNV, FCMEN, and FCMSE results.

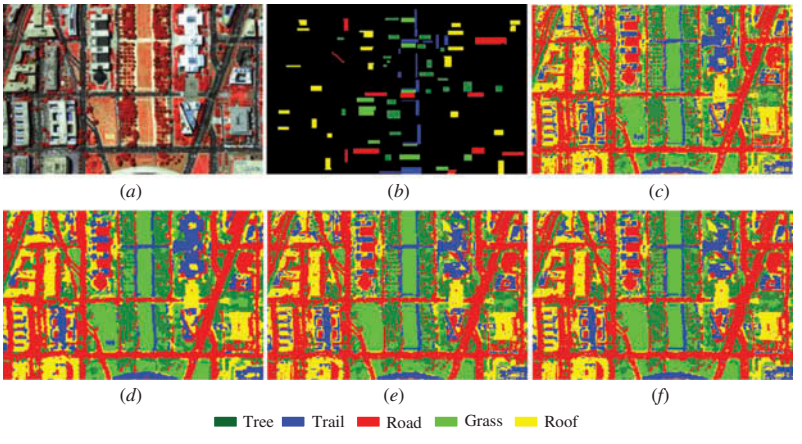

Figure 2. Results of HYDICE data set. (*a*) Three-band colour composite image (bands 65, 52, and 36 as RGB). (*b*) Ground truth. (*c*)–(*f*) FCM, FCMNV, FCMEN, and FCMSE results.

test samples of tree, trail, road, grass, and roof are 1135, 908, 1175, 891, and 1378, respectively.

The Reflective Optics System Imaging Spectrometer (ROSIS) data set. The data set was acquired by the ROSIS sensor during a flight campaign over the University of Pavia, Italy. The data set has 103 bands and a spatial resolution of 1.3 m (Wang and Wang 2013). A region with 256 × 256 pixels was studied, which mainly contains five classes of interest: asphalt, meadow, brick, tree, and metal sheet. The corresponding numbers of test samples for the five classes are 2810, 3263, 1276, 1220, and 1371. The three-band colour image and ground truth are shown in figures 3(*a*) and (*b*).

4.2 *Results*

In the experiments for FCM, the number of clusters was set to 4, 5, and 5 for the FLC1, HYDICE, and ROSIS data sets, respectively. For two UAFCM algorithms (i.e., FCMEN and FCMSE), ρ was set to 1. The neighbourhood window size in FCMEN, FCMSE, and FCMNV is set to 3 × 3 (i.e., $W = 3$). The unsupervised classification results of FCM, FCMNV, FCMEN, and FCMSE for three images are shown in figures 1(*c*)–(*f*), 2(*c*)–(*f*), and 3(*c*)–(*f*).

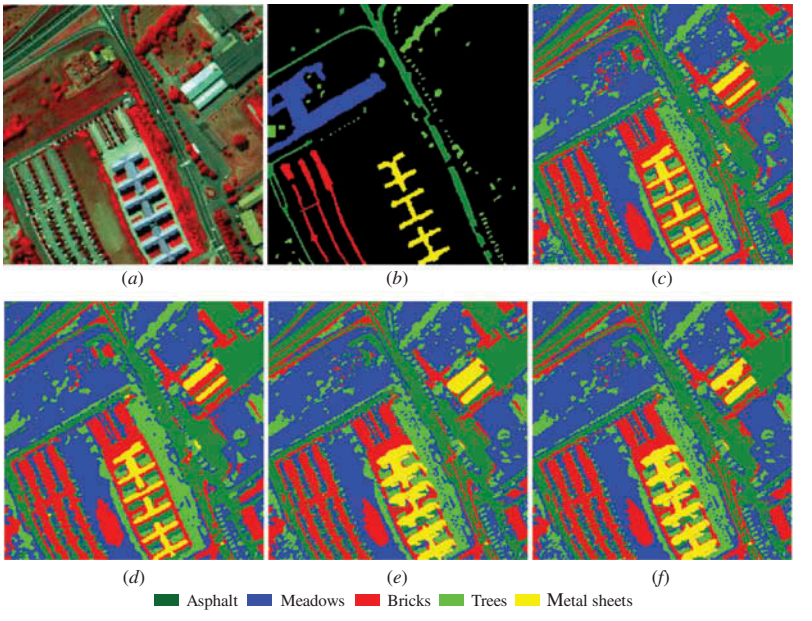

Figure 3. Results of ROSIS data set. (*a*) Three-band colour composite image (bands 90, 60, and 40 as RGB). (*b*) Ground truth. (*c*)–(*f*) FCM, FCMNV, FCMEN, and FCMSE results.

As can be observed from the results of three classification methods, two UAFCM-based classifiers FCMEN and FCMSE can provide better results than FCM and FCMNV. There are many incorrectly classified and isolated pixels in FCM results. Though FCMNV can enhance FCM by removing scattering of pixels in FCM maps, its performance is still poorer than FCMEN and FCMSE in general. Specifically, in FLC1 data set results, there are obvious isolated pixels in FCM result and many pixels that should be classified as wheat and oats are labelled as soy. With FCMNV, these isolated pixels are almost eliminated, but some pixels for soy are still incorrectly classified as soy. In FCMEN and FCMSE results, however, by reclassification of pixels with large uncertainty, the misclassification has been noticeably alleviated and the classification of wheat and oats is more satisfying. For unsupervised classification of the HYDICE and ROSIS data sets, FCM yields a number of isolated pixels again. FCMNV shows its advantage in classification of roof and tree in the HYDICE image, but yield over-smoothed results of ROSIS image. Both FCMEN and FCMSE outperform FCM from visual inspection. This can be well illustrated by the classification of road and grass in the HYDICE data set and meadow in the ROSIS data set. The visual comparison evidently validates the advantage of the proposed UAFCM in classification.

The advantage of the proposed UAFCM is also confirmed quantitatively by classification accuracy in terms of the percentage of correctly classified pixels. Table 1 lists the overall accuracy (OA) for FCM, FCMNV, FCMEN, and FCMSE for three data sets. For classification of FLC1 data set, the classification accuracy of both FCMEN and FCMSE is higher than that of FCM and FCMNV. The OA of FCMEN is 4.42%, 3.81%, and 0.56% greater than that of FCM, FCMNV, and FCMSE. For HYDICE data set, FCMNV, FCMEN, and FCMSE are competent in classification and all of them are superior to FCM. As for the ROSIS data set, the OA of the proposed FCMEN and FCMSE is higher than the other two methods. Moreover, FCMSE

Table 1. OA (%) of unsupervised classifiers for three images.

	FCM	FCMNV	FCMEN	FCMSE
FLC1	84.07	84.68	88.49	87.93
HYDICE	72.94	75.93	75.94	76.03
ROSIS	91.44	93.11	94.26	94.66

obtains slightly higher accuracy than FCMEN, with gains of 3.22% and 1.55% over FCM and FCMNV respectively.

To evaluate the statistical significance in accuracy for different unsupervised classifiers, McNemar's test (Foody 2004) was also applied. Using the 95% degree of confidence level, the McNemar's test results indicate FCMNV and two UAFCM-based classifiers (i.e., FCMEN and FCMSE) provide significantly higher accuracy than FCM classifier for all three images. With respect to comparison between FCMNV and UAFCM, the latter tends to achieve significantly higher accuracy. The inter-comparison between FCMSE and FCMEN reveals that the two UAFCM-based classifiers are generally competent in classification.

The proposed FCMEN and FCMSE were also compared with a MRF-based unsupervised classifier. The MRF-based discriminant function for class i ($i = 1, 2, \ldots, k$) on pixel $\boldsymbol{x}_j$ ($j = 1, 2, \ldots, n$) is expressed as follows:

$$g_i(\boldsymbol{x}_j) = \frac{1}{N}\sum_{t=1}^{N} \beta\delta(i, \boldsymbol{x}_t) + (1-\beta)u_{ij} \tag{12}$$

where $\beta \in (0,1)$ is a control parameter, N is the number of neighbouring pixels, and $\delta(i, \boldsymbol{x}_t)$ is a function that counts the number of neighbouring pixels belonging to class i. The spectral term of the MRF model in equation (12) is calculated by FCM. In this letter, a simple and fast approach based on Besag's iterated conditional modes (ICMs) algorithm was applied to generate classification results for MRF model (Bruzzone and Prieto 2000). The parameter β controls the contributions from spatial and spectral terms (Wang and Wang 2013) and plays an important role in MRF-based classification approach. It was tested from 0.1 to 0.9 with a step of 0.1, as exhibited in figure 4. It can be observed that two UAFCM methods, overall, achieve higher OA than does MRF for classification of the FLC1 and ROSIS data set. As for the HYDICE data set, only when β is greater than 0.7, MRF is able to obtain more accurate result.

The parameter ρ in equation (11) determines the threshold used to recognize pixels with large uncertainty. Its influence on the two UAFCM algorithms was analysed. Specifically, ρ was tested for the three data sets from 0 to 2 with a step of 0.1, as shown in figure 5. It is worth noting that the accuracy of FCMEN and FCMSE takes the same tendency when ρ varies and the two methods are competent in classification in general. When ρ is large enough, the accuracy of both FCMSE and FCNEN becomes the same as that of FCM. This is because the threshold is over large and none pixels can be recognized as uncertain ones. When ρ takes values between 0.5 and 1.5, UAFCM can enhance. With $\rho = 1$, two UAFCM algorithms are able to achieve relatively high classification accuracy and the corresponding OA is higher than that of FCM and FCMNV, suggesting $\rho = 1$ is an effective choice for determination of threshold in equation (11).

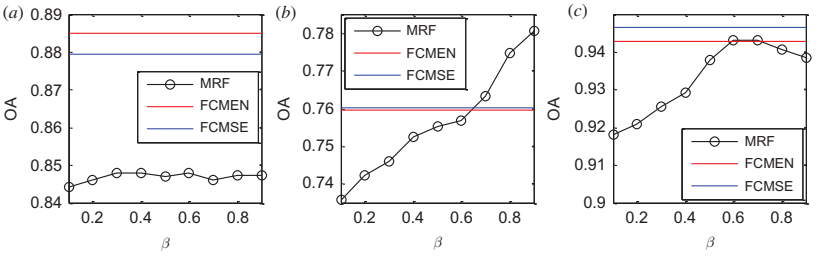

Figure 4. Comparing UAFCM with MRF-based unsupervised classification for three data sets with varying parameter β. (*a*) The FLC1 data set. (*b*) The HYDICE data set. (*c*) The ROSIS data set.

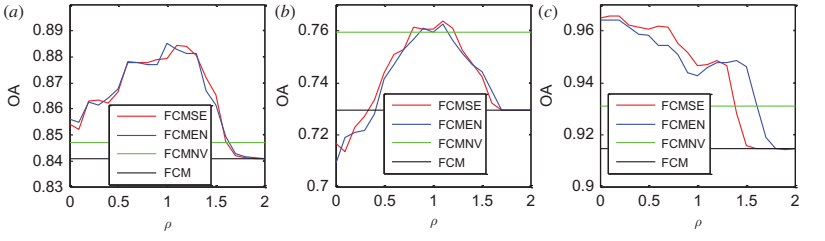

Figure 5. Influence of ρ for UAFCM. (*a*) The FLC1 data set. (*b*) The HYDICE data set. (*c*) The ROSIS data set.

5. Conclusions

A new classification method, UAFCM, is introduced in this letter. UAFCM is a post-processing of traditional FCM classification. The new method is realized by reclassifying those pixels with large uncertainty in FCM classification result. The uncertainty is measured by entropy and the proposed square error-based criterion. Then, a threshold value is determined according to measured uncertainty for all pixels in the studied remote sensing image. By comparing to the threshold value, uncertain pixels in FCM classification are recognized and reclassified with spatial connectivity at last. Three data sets were tested for validation of UAFCM. From both visual and quantitative assessment, it is shown that UAFCM with uncertainty measured by entropy and the proposed square error (i.e., FCMEN and FCMSE) can enhance FCM. Furthermore, UAFCM is capable of obtaining better results than FCMNV and the MRF-based unsupervised classification approach. Future work will focus on developing other methods of reclassification of pixels with large uncertainty.

Acknowledgements

This work was supported by Research Grants Council, Hong Kong (PolyU 5249/12E) and the Hong Kong Polytechnic University (Project No.: 1-ZV4F, 1-ZVBA, G-U753, G-UA35, G-YK75, G-YJ75, G-YZ26, and H-ZG77). The authors would like to thank Professor D. Landgrebe, Purdue University, West Lafayette, IN, USA, for providing the FLC1 and HYDICE data set, Professor Paolo Gamba of the University of Pavia for providing the ROSIS data, and Dr. Lefei Zhang of the Wuhan University for providing the ground truth of the HYDICE data set. The reviewers' valuable suggestions and comments have greatly improved this manuscript.

References

Bagan, H., Wang, Q., Watanabe, M., Yang, Y. and Ma, J., 2005, Land cover classification from MODIS EVI times-series data using SOM neural network. *International Journal of Remote Sensing*, **26**, pp. 4999–5012.

Bandyopadhyay, S., Maulik, U. and Mukhopadhyay, A., 2007, Multiobjective genetic clustering for pixel classification in remote sensing imagery. *IEEE Transactions on Geoscience and Remote Sensing*, **45**, pp. 1506–1511.

Bezdek, J.C., 1981, *Pattern Recognition with Fuzzy Objective Function Algorithms* (New York: Plenum Press).

Brown, K.M., Foody, G.M. and Atkinson, P.M., 2009, Estimating per-pixel thematic uncertainty in remote sensing classifications. *International Journal of Remote Sensing*, **30**, pp. 209–229.

Bruzzone, L. and Prieto, D.F., 2000, Automatic analysis of the difference image for unsupervised change detection. *IEEE Transactions on Geoscience and Remote Sensing*, **38**, pp. 1171–1182.

Dehghan, H. and Ghassemian, H., 2006, Measurement of uncertainty by the entropy: application to the classification of MSS data. *International Journal of Remote Sensing*, **27**, pp. 4005–4014.

Dopido, I., Villa, A., Plaza, A. and Gamba, P., 2006, A quantitative and comparative assessment of unmixing-based feature extraction techniques for hyperspectral image classification. *IEEE Journal of Selected Topics in Applied Earth Observation and Remote Sensing*, **5**, pp. 421–435.

Duda, R.O., Hart, P.E. and Stork, D.G., 2001, *Pattern Classification* (2nd ed.) (New York: Wiley).

Evans, A.N. and Nixon, M.S., 1995, Mode filtering to reduce ultrasound speckle for feature extraction. *IEEE Proceedings – Vision Image and Signal Processing*, **142**, pp. 87–94.

Foody, G.M., 1995, Cross-entropy for the evaluation of the accuracy of a fuzzy land cover classification with fuzzy ground data. *ISPRS Journal of Photogrammetry and Remote Sensing*, **50**, pp. 2–12.

Foody, G.M., 2004, Thematic map comparison evaluating the statistical significance of differences in classification accuracy. *Photogrammetric Engineering and Remote Sensing*, **70**, pp. 627–633.

Hall, D. and Ball, G., 1965, *ISODATA: A Novel Method of Data Analysis and Pattern Classification*. Technical report (Menlo Park, CA: Stanford Research Institute).

Richards, J.A. and Jia, X., 2006, *Remote Sensing Digital Image Analysis* (3rd ed.) (Berlin: Springer-Verlag).

Senthilnath, J., Omkar, S.N., Mani, V., Karnwal, N. and Shreyas, P.B., 2013, Crop stage classification of hyperspectral data using unsupervised techniques. *IEEE Journal of Selected Topics in Applied Earth Observation and Remote Sensing*, **6**, pp. 861–868.

Wang, L. and Wang, Q., 2013, Subpixel mapping using Markov random field with multiple spectral constraints from subpixel shifted remote sensing images. *IEEE Geoscience and Remote Sensing Letters*, **10**, pp. 598–602.

Wang, Q., Wang, L. and Liu, D., 2012, Particle swarm optimization-based sub-pixel mapping for remote-sensing imagery. *International Journal of Remote Sensing*, **33**, pp. 6480–6496.

Xu, K., Yang, W., Liu, G. and Sun, H., 2013, Unsupervised satellite image classification using Markov field topic model. *IEEE Geoscience and Remote Sensing Letters*, **10**, pp. 130–134.

Zhang, L., Zhang, L., Tao, D. and Huang, X., 2013, Tensor discriminative locality alignment for hyperspectral image spectral–spatial feature extraction. *IEEE Transactions on Geoscience and Remote Sensing*, **51**, pp. 242–256.

Zhong, Y., Zhang, L. and Li, P., 2011, Unsupervised remote sensing image classification using an artificial immune network. *International Journal of Remote Sensing*, **32**, pp. 5461–5483.